© Journal for Modeling in Ophthalmology 2017;4:16-28
Original article

FIRE: Fundus Image Registration dataset

Carlos Hernandez-Matas[1,2], Xenophon Zabulis[1], Areti Triantafyllou[3], Panagiota Anyfanti[3], Stella Douma[3], Antonis A. Argyros[1,2]

[1]*Institute of Computer Science, Foundation for Research and Technology – Hellas (FORTH), Heraklion, Greece*, [2]*Computer Science Department, University of Crete, Heraklion, Greece*, [3]*3rd Department of Internal Medicine, Papageorgiou Hospital, Aristotle University of Thessaloniki, Thessaloniki, Greece*

Abstract

Purpose: Retinal image registration is a useful tool for medical professionals. However, evaluating the accuracy of these registration methods has not been consistently undertaken in the literature. To address this, a dataset comprised of retinal image pairs annotated with ground truth and an evaluation protocol for registration methods is proposed.
Methods: The dataset is comprised of 134 retinal fundus image pairs. These pairs are classified into three categories, according to characteristics that are relevant to indicative registration applications. Such characteristics are the degree of overlap between images and the presence/absence of anatomical differences. Ground truth in the form of corresponding image points and a protocol to evaluate registration accuracy are provided.
Results: Using the aforementioned protocol, it is shown that the Fundus Image Registration (FIRE) dataset enables quantitative and comparative evaluation of retinal registration methods under a variety of conditions.
Conclusion: This work enables the fair comparison of retinal registration methods. It also helps researchers to select the registration method that is most appropriate given a specific target use.

Keywords: benchmark, dataset, evaluation, retinal fundus images, retinal image registration

Correspondence: Institute of Computer Science, Foundation for Research and Technology – Hellas (FORTH), N. Plastira 100, Vassilika Vouton, GR-700 13 Heraklion, Crete, Greece.
E-mail: carlos@ics.forth.gr

1. Introduction

Fundoscopy enables non-invasive observation of the microvascular circulation.[1] Diagnosis and monitoring of diseases with commonly observed vasculopathy, such as diabetes and hypertension,[2] can be assisted with the assessment of microcirculation by measuring and monitoring vascular morphology. Image registration[3–5] – a tool whose aim is to warp a test image to the coordinate frame of a reference image so that the same point is imaged at the same coordinates in both images – can be of great assistance for this task for several applications in retinal imaging. Such applications include super resolution,[6–8] mosaicing,[9–11] and longitudinal studies.[12,13]

The image pairs involved in each of these applications exhibit different characteristics. In super resolution, images with a large overlapping surface can be combined to create images of higher resolution and definition which, in turn, allow for more accurate measurements. Stitching images into mosaics provides images with a larger field of view (FOV) that image a greater area of the retinal surface, and is usually possible even when the overlap of the input images is small. In longitudinal studies, disease progression or regression can be monitored employing images from different examination sessions.

In addition to being of interest and of practical significance, the registration of retinal images is a challenging problem. Image pairs can present illumination, color, and contrast changes, as well as potentially small overlapping areas. Additionally, there might be structural changes in the retina due to the progression or remission of retinopathy. The support of medical diagnosis requires accurate measurements. This calls for methods, datasets, and protocols for quantifying the accuracy of retinal image analysis methods.[14]

In this work, a benchmark dataset for the evaluation of retinal image registration methods is introduced. The dataset consists of image pairs that are annotated with ground truth for their registration in the form of point correspondences between them. In addition, a protocol for the quantitative assessment of the accuracy of retinal image registration methods as well as their comparative evaluation is suggested. The dataset could also be utilized for other purposes, such as vessel segmentation and optic disc feature analysis or diagnosis, potentially in a comparative way due to the registration of images. However, no ground truth is provided for any other purpose besides retinal image registration.

2. Related work

Numerous publicly available datasets exist containing retinal images. They have been compiled for different purposes such as segmentation of diverse elements of the retina (CHASEDB1,[15,16] DRIONS-DB,[17,18] Drishti-GS,[19,20] DRIVE,[21,22] HRF,[23,24] MESSIDOR,[25,26] ONHSD,[27,28] and REVIEW[29,30]), diagnosis (DIARETDB0,[31,32] ROC,[33,34] DIARETDB1,[35,36] e-ophtha,[37,38] STARE,[39,40] INSPIRE-AVR,[41,42] and VICAVR[43,44]), user authentication (VARIA[45,46]) and retinal image registration (FIRE[47] and RODREP[48,49]).

Table 1 shows a list of technical characteristics pertaining these datasets. Apart from e-ophtha, FIRE, VARIA, and RODREP, the rest of the datasets are not useful for the purpose of performing retinal image registration, as they do not provide pairs of retinal images.

Table 1. Publicly available retinal image datasets

Dataset	Images	Field of view	Resolution	Registrable image pairs
CHASEDB1[15,16]	14	$\approx 25^\circ$	999×960	0
DIARETDB0[31,32]	130	50°	1500×1152	0
DIARETDB1[35,36]	89	50°	1500×1152	0
DRIONS-DB[17,18]	110	$\approx 30^\circ$	600×400	0
Drishti-GS[19,20]	101	$\approx 25^\circ$	2045×1752	0
DRIVE[21,22]	40	45°	565×584	0
e-ophtha[37,38]	463	$\approx 45^\circ$	2544×1696	144
FIRE[47]	129	45°	2912×2912	134
HRF[23,24]	45	45°	3504×2336	0
INSPIRE-AVR[41,42]	40	30°	2392×2048	0
MESSIDOR[25,26]	1200	45°	1440×960 – 2304×1536	0
ONHSD[27,28]	99	45°	640×480	0
REVIEW[29,30]	14	$\approx 45^\circ$	1360×1024 – 3584×2438	0
ROC[33,34]	100	$\approx 30^\circ$ – 45°	768×576 – 1386×1391	0
RODREP[48,49]	1120	45°	2000×1312	≈ 1400
STARE[39,40]	397	$\approx 30^\circ$ – 45°	700×605	0
VARIA[45,46]	233	20°	768×584	154
VICAVR[43,44]	58	45°	768×584	0

The RODREP dataset provides a large amount of images retrieved following a screening program in which two sets of four pictures were acquired for 140 eyes. There is very limited overlap in these sets of four images, as the purpose is to generate a mosaic from the images. Given the characteristics of the screening, we estimate that for each eye there are approximately ten image pairs: three pairs from the same session for each of the two sessions, and four pairs with an image from each session. This totals 1400 image pairs in the dataset. While the amount of images and possible image pairs is impressive, we consider the dataset lacking in two respects, as far as image registration is concerned. First, there are no image pairs in which, due to progression or remission of illness, large anatomical differences exist in the retina. Some of these changes may correspond to microaneurysms, cotton-wool spots, hard exudates, and other forms of retinopathy resulting from illnesses such as hypertension and diabetes. Registration of these kinds of images is key in clinical practice for the better study of retinopathy progression. Additionally, these differences may

prove very challenging for automatic registration methods. Second, the dataset lacks ground truth information. Ground truth is critical to quantitatively evaluate the accuracy of a registration method. The RODREP authors rely on visual inspection by medical experts to grade the registration accuracy of their method.[48] This is a time-consuming task for medical experts to the extent that, as reported, some of them did not complete the task.

The e-ophtha dataset provides several image pairs, both with large and small overlaps of the retina. However, in a similar fashion to RODREP, there are no image pairs with anatomical differences, and no ground truth is provided.

VARIA also provides several image pairs. However, the FOV of the images is small, all the image pairs have a large overlapping area of the retina, and no ground truth is provided. Thus, this dataset is quite limited for the purpose of retinal image registration.

The contributions of this work are the following. The FIRE retinal image dataset is introduced. A protocol for quantitative and comparative accuracy evaluation of retinal image registration methods is suggested. Compared to the aforementioned works, the FIRE dataset exhibits the following advantages. The dataset is comprised of registrable image pairs, annotated with ground truth for image registration. Ground truth is provided in the form of point correspondences between image pairs.

In addition, FIRE is divided into three categories, making it suitable for the evaluation of registration methods that address diverse application scenarios.

3. The FIRE dataset

The FIRE dataset (publicly available at: http://www.ics.forth.gr/cvrl/fire) contains several retinal image pairs with the aim of assessing the accuracy of retinal image registration. Two binary mask images are also included. The first distinguishes the pixels that contain color information from the ones that correspond to the black, circular frame of the image. This information is useful for global registration methods. The second mask marks a proposed area, suitable for finding corresponding points. This is useful for local registration methods. The images in each pair are in `.jpg` format, and are the original images acquired from the imaging device. The masks are provided in `.png` format. Additionally, ground truth image point correspondences are provided for each image pair, so that they can be used to validate the accuracy of an image registration algorithm. These correspondences are provided in `.txt` files, one for each image pair.

3.1 Retinal images

FIRE consists of a collection of 129 retinal images forming 134 image pairs. For a single eye there might be several images, therefore, several image pair combinations can be formed. The images were acquired with a Nidek AFC-210 fundus camera, which has a resolution of 2912×2912 pixels and a FOV of $45^\circ \times 45^\circ$. Images were acquired at the

Hypertension Unit of the 3rd Department of Internal Medicine, Papageorgiou Hospital, Aristotle University of Thessaloniki, Greece, from 39 female and male patients aged 19-67 who attended their regular appointments between 2006 and 2015. Written informed consent was obtained before data acquisition and processing.

The image pairs are classified into three categories depending on the characteristics of the pairs. Each pair is a member of a single category.

Category $\mathcal{S}$ contains 71 image pairs. Images defining a pair exhibit a large spatial overlap (> 75%) and lack visual anatomical differences. This provides images that after registration could be useful for performing super resolution.

Category $\mathcal{P}$ contains 49 image pairs. Again, images defining a pair lack visual anatomical differences. However, they exhibit a smaller overlap than category $\mathcal{S}$ (< 75%). These type of image pairs could be useful for mosaicing applications.

Category $\mathcal{A}$ contains 14 image pairs with a large overlap. The images in a specific pair are acquired at different examinations. Moreover, they feature visual anatomical differences due to the progression or remission of retinopathy. These differences may appear in the form of increased vessel tortuosity, microaneurysms, cotton-wool, spots, etc. Such changes typically occur in longitudinal studies.

Categories $\mathcal{S}$ and $\mathcal{P}$ also include pathological cases that may affect the structure of the retina, but as the images lack anatomical differences, retinopathy remains unchanged among the images in each pair. All three categories may feature eye shape deformations caused by myopia, hypermetropia, and similar conditions. Category characteristics are summarized in Table 2.

Table 2. Characteristics of the FIRE dataset image pair categories

	Category $\mathcal{S}$	**Category $\mathcal{P}$**	**Category $\mathcal{A}$**
# Image pairs	71	49	14
Approximate overlap	> 75%	< 75%	> 75%
Anatomical changes	No	No	Yes
Indicative registration application	Super Resolution	Mosaicing	Longitudinal Study

Figure 1 shows sample image pairs from the three categories. The leftmost column shows a pair from Category $\mathcal{S}$. The second column shows a pair from Category $\mathcal{P}$. In column 3, there is a pair from Category $\mathcal{A}$ in which the test image exhibits anatomical differences compared to the reference image, such as increased vessel tortuosity, cotton-wool spots, and hemorrhages. The rightmost column shows another pair from Category $\mathcal{A}$, in which the test image exhibits additional hemorrhages, cotton-wool spots, and vessel thinning, compared to the reference image.

3.2 Ground truth

In the relevant literature, the assessment of an image registration method is performed based on several quantitative and qualitative approaches. Quantitative ap-

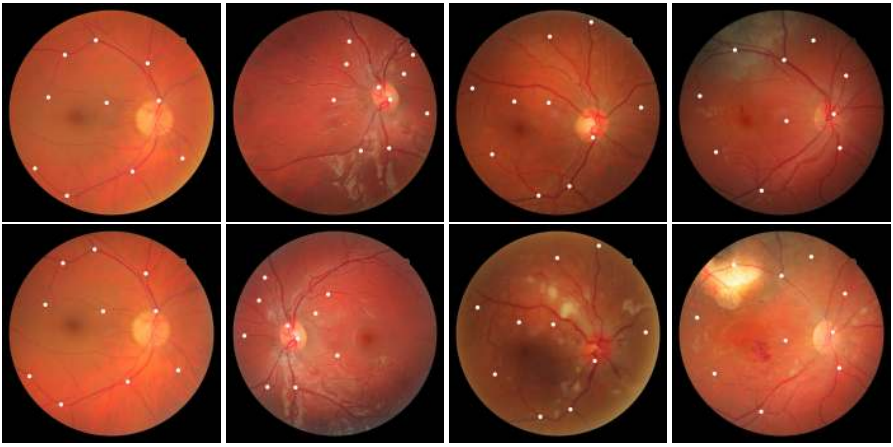

Fig. 1. Image pairs from the FIRE dataset. Leftmost column shows a pair from Category $\mathcal{S}$, the second column a pair from Category $\mathcal{P}$, and the two rightmost pairs from Category $\mathcal{A}$. White dots indicate control point locations.

proaches include the utilization of manually[50–55] or automatically[56–58] selected control points. This has the advantage of reporting registration error as a single number. Other quantitative approaches[59–62] estimate the transformation (scaling, rotation, and translation) that governs the solution provided by a method. A similar transformation is estimated for the ground truth solution that is approved by an expert. The two transformations are then compared. However, this solution usually provides the error as a collection of several parameters. Qualitative approaches usually focus on visual supervision of vessel alignment in images,[48] such as counting the amount and measuring the magnitude of discontinuities on a checkerboard superimposition after registration.[63] This task is time-consuming, requires the involvement of an expert, and does not allow for quantitative comparison between registration methods.

In the proposed dataset, we provide ground truth for the calculation of the registration error in the form of corresponding points between the images in the pair. These are henceforth referred to as control points. The location of a control point j in the reference image is denoted as $\mathbf{c}_j$, and the corresponding point in the test image as $\mathbf{t}_j$. A registration method takes the points $\mathbf{t}_j$ as input and maps them to the new coordinates $\mathbf{r}_j$. Thus, the $\mathbf{r}_j$ points are the $\mathbf{t}_j$ points after registration. If registration is perfect, points $\mathbf{c}_j$ and $\mathbf{r}_j$ coincide and their distance (in image pixels) is 0.

Ten corresponding points are provided for each image pair. An annotator manually selected these correspondences, locating approximately eight of them towards the edges of the overlapping area and the remaining points towards the center. Points were chosen to be widespread across the image, providing a broad coverage of the overlapping surface between images, so that the accuracy across the whole image can be calculated. Given that they were manually selected, points are mainly located on vessels and crossings as they allowed the annotator to provide accurate initial

markings, which is a challenging task with uncertain outcome in other image areas that lack image structure. The amount of correspondences was selected by balancing the trade-off between time availability of the annotator, accuracy of annotations, and number of marked images.

The effect of human error in the location of the correspondences is mitigated using computational methods as follows. For each corresponding pair of points $\mathbf{c}_j$ and $\mathbf{t}_j$, a grid of neighboring points $\mathbf{n}_{c,j}$ and $\mathbf{n}_{t,j}$ was considered. Image patches $s_{c,j}$ and $s_{t,j}$ centered around each $\mathbf{n}_{c,j}$ and $\mathbf{n}_{t,j}$ were created. The points $\mathbf{n}_{c,j}$ and $\mathbf{n}_{t,j}$ with the highest correlation between $s_{c,j}$ and $s_{t,j}$ were chosen as $\mathbf{c}_j$ and $\mathbf{t}_j$. The locations of control points for four image pairs of the FIRE dataset are shown in Figure 1.

The refined control points are independent from widely employed automatic feature selection methods such as Scale-Invariant Feature Transform[64] (SIFT) and Speeded Up Robust Features[65] (SURF). This prevents bias in evaluating registration methods based on such features.

4. Registration evaluation

In this section, we suggest a method to evaluate the accuracy of a given retinal image registration method that allows for simple comparison with other competing methods. We use a conventional measure of the registration error for an image pair, that is, the mean distance between all $\mathbf{c}_j$ and $\mathbf{r}_j$ in the pair. To evaluate the registration accuracy of a method across a dataset, we focused on relevant efforts in the field of evaluating object tracking methods,[66] specifically by employing a 2D plot. The x axis of the plot corresponds to the value of an error threshold. If the registration error of an image pair is below this threshold, the registration is considered successful. The y axis of the plot corresponds to the percentage of successfully registered image pairs for a given threshold. This creates a continuous monotonic curve which shows success rate as a function of target accuracy. Thus, the selection of an arbitrary threshold is avoided. Moreover, a registration method can be selected based on the accuracy requirements of the intended application. We use such plots to show registration accuracy for each individual category, as well as for the whole FIRE dataset.

By considering a variety of target registration accuracies, this measure facilitates the comparison of competing methods and the selection of the most appropriate one, given the registration accuracy requirements of a certain application. For example, in Figure 2 the registration accuracy for both GDB-ICP[67] and the Hernandez-Matas *et al.* method[58] is shown. It can easily be verified that the Hernandez-Matas *et al.* method always performs better than GDB-ICP in categories $\mathcal{S}$ and $\mathcal{A}$. The GDB-ICP method is preferable for image pairs in category $\mathcal{P}$ up to a certain error threshold.

Making the registration error for each image pair publicly available is encouraged to facilitate comparison between different registration methods. The registration errors for the methods in Figure 2 are available at: http://www.ics.forth.gr/cvrl/fire. The aim is to create a repository where results obtained by other methods are included as they become available.

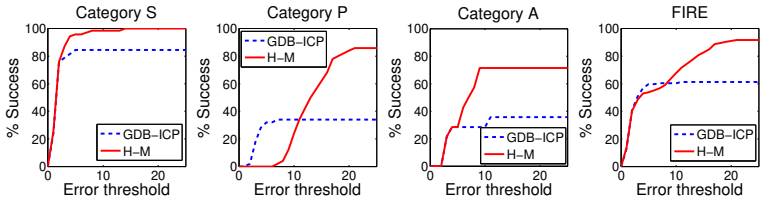

Fig. 2. Registration success for GDB-ICP[67] and the Hernandez-Matas *et al.* method.[58] The x axis marks the registration error threshold under which a registration is considered to be successful. The y axis marks the percentage of successfully registered image pairs for a given threshold.

5. Discussion

FIRE consists of three categories of retinal image pairs. Each category is compiled with the intention of covering a different challenge in retinal image registration. For each image pair, ground truth information in the form of control points is provided.

Table 3 shows a comparison between the e-ophtha, FIRE, RODREP, and VARIA datasets. While e-ophtha, RODREP, and VARIA present more standalone images and registrable image pairs, FIRE provides a wider range of scenarios, higher-resolution images, and most importantly, ground truth information, which is of paramount importance for the quantitative and, thus, objective assessment of registration accuracy.

Table 3. Characteristics of image pairs in e-ophtha, FIRE, RODREP, and VARIA

Dataset	**Images**	**Field of view**	**Resolution**	**Registrable image pairs**
e-ophtha[37,38]	463	$\approx 45^\circ$	2544×1696	144
FIRE[47]	129	45°	2912×2912	134
RODREP[48,49]	1120	45°	2000×1312	≈ 1400
VARIA[45,46]	233	20°	768×584	154
	Large overlap	**Small overlap**	**Anatomical differences**	**Registration ground truth**
e-ophtha[37,38]	Yes	Yes	No	No
FIRE[47]	Yes	Yes	Yes	Yes
RODREP[48,49]	Yes	Yes	No	No
VARIA[45,46]	Yes	No	No	No

We believe that the introduction of the FIRE dataset is a valuable contribution to the retinal image registration community, as it provides data to perform fair comparisons between retinal registration methods with different end applications in mind. Moreover, the suggested evaluation measure may assist researchers and/or practitioners in need of a registration method to select the one that best suits their needs.

Acknowledgments

This research was made possible by a Marie Curie grant from the European Commission in the framework of the REVAMMAD ITN (Initial Training Research Network), Project number 316990. It was also supported by the FORTH-ICS internal RTD Program "Ambient Intelligence and Smart Environments". Authors would like to thank the anonymous reviewers for their invaluable feedback.

References

1. Abramoff MD, Garvin MK, Sonka M. Retinal Imaging and Image Analysis. IEEE Reviews in Biomedical Engineering, 2010;3, 169–208. ISSN: 1937-3333. doi: 10.1109/RBME.2010.2084567.
2. Grosso A, Veglio F, Porta M, Grignolo FM, Wong TY. Hypertensive retinopathy revisited: some answers, more questions. British Journal of Ophthalmology, 2005;89(12): 1646–1654. doi: 10.1136/bjo.2005.072546.
3. Hill DLG, Batchelor PG, Holden M, Hawkes DJ. Medical image registration. Physics in Medicine and Biology, 2001;46(3): R1. Available from: http://stacks.iop.org/0031-9155/46/i=3/a=201.
4. Sotiras A, Davatzikos C, Paragios N. Deformable Medical Image Registration: A Survey. Research Report (RR-7919): INRIA, Sept. 2012; Available from: https://hal.inria.fr/hal-00684715.
5. Oliveira FP, Tavares JMR. Medical image registration: a review. Computer Methods in Biomechanics and Biomedical Engineering, 2014;17(2): PMID: 22435355, 73–93. doi: 10.1080/10255842.2012.670855.
6. Meitav N, Ribak EN. Improving retinal image resolution with iterative weighted shift-and-add. Journal of the Optical Society of America A, July 2011;28(7): 1395–1402. doi: 10.1364/JOSAA.28.001395.
7. Hernandez-Matas C, Zabulis X. Super resolution for fundoscopy based on 3D image registration. 2014 36th Annual International Conference of the IEEE Engineering in Medicine and Biology Society. Aug. 2014; 6332–6338. doi: 10.1109/EMBC.2014.6945077.
8. Molodij G, Ribak E, Glanc M, Chenegros G. Enhancing retinal images by extracting structural information. Optics Communications, 2014;313, 321 –328. ISSN: 0030-4018. doi: 10.1016/j.optcom.2013.10.011.
9. Can A, Stewart CV, Roysam B, Tanenbaum HL. A feature-based technique for joint, linear estimation of high-order image-to-mosaic transformations: mosaicing the curved human retina. IEEE Transactions on Pattern Analysis and Machine Intelligence, Mar. 2002;24(3): 412–419. ISSN: 0162-8828. doi: 10.1109/34.990145.
10. Ryan N, Heneghan C, Chazal P de. Registration of digital retinal images using landmark correspondence by expectation maximization. Image and Vision Computing, 2004;22(11): 883 –898. ISSN: 0262-8856. doi: 10.1016/j.imavis.2004.04.004.
11. Cattin PC, Bay H, Van Gool L, Székely G. Retina Mosaicing Using Local Features. Medical Image Computing and Computer-Assisted Intervention – MICCAI 2006: 9th International Conference, Copenhagen, Denmark, October 1-6, 2006. Proceedings, Part II. Ed. by R Larsen, M Nielsen, J Sporring. Berlin, Heidelberg: Springer Berlin Heidelberg, 2006; 185–192. ISBN: 978-3-540-44728-3. doi: 10.1007/11866763_23.
12. Narasimha-Iyer H, Can A, Roysam B, Tanenbaum HL, Majerovics A. Integrated Analysis of Vascular and Nonvascular Changes From Color Retinal Fundus Image Sequences. IEEE Transactions on Biomedical Engineering, Aug. 2007;54(8): 1436–1445. ISSN: 0018-9294. doi: 10.1109/TBME.2007.900807.
13. Troglio G, Alberti M, Benediksson JA, Moser G, Serpico SB, Stefánsson E. Unsupervised Change-Detection in Retinal Images by a Multiple-Classifier Approach. Multiple Classifier Systems: 9th International Workshop, MCS 2010, Cairo, Egypt, April 7-9, 2010. Proceedings. Ed. by N El Gayar, J Kittler, F Roli. Berlin, Heidelberg: Springer Berlin Heidelberg, 2010; 94–103. ISBN: 978-3-642-12127-2. doi: 10.1007/978-3-642-12127-2_10.

14. Trucco E, Ruggeri A, Karnowski T, Giancardo L, Chaum E, Hubschman JP, et al. Validating Retinal Fundus Image Analysis Algorithms: Issues and a ProposalValidating Retinal Fundus Image Analysis Algorithms. Investigative Ophthalmology & Visual Science, 2013;54(5): 3546. doi: 10.1167/iovs.12-10347.
15. Fraz MM, Remagnino P, Hoppe A, Uyyanonvara B, Rudnicka AR, Owen CG, et al. An Ensemble Classification-Based Approach Applied to Retinal Blood Vessel Segmentation. IEEE Transactions on Biomedical Engineering, 2012;59(9): 2538–2548. ISSN: 0018-9294. doi: 10.1109/TBME.2012.2205687.
16. CHASEDB1 Retinal Image Database. [Accessed June 8, 2017]. Available from: https://blogs.kingston.ac.uk/retinal/chasedb1/.
17. Carmona EJ, Rincón M, García-Feijoó J, Casa JM Martínez-de-la. Identification of the Optic Nerve Head with Genetic Algorithms. Artificial Intelligence in Medicine, July 2008;43(3): 243–259. ISSN: 0933-3657. doi: 10.1016/j.artmed.2008.04.005.
18. DRIONS-DB: Digital Retinal Images for Optic Nerve Segmentation Database. [Accessed June 08, 2017]. Available from: http://www.ia.uned.es/~ejcarmona/DRIONS-DB.html.
19. Sivaswamy J, Krishnadas SR, Joshi GD, Jain M, Tabish AUS. Drishti-GS: Retinal image dataset for optic nerve head(ONH) segmentation. 2014 IEEE 11th International Symposium on Biomedical Imaging (ISBI). 2014; 53–56. doi: 10.1109/ISBI.2014.6867807.
20. Drishti-GS Dataset. [Accessed June 08, 2017]. Available from: http://cvit.iiit.ac.in/projects/mip/drishti-gs.
21. Staal J, Abramoff MD, Niemeijer M, Viergever MA, Ginneken B van. Ridge-based vessel segmentation in color images of the retina. IEEE Transactions on Medical Imaging, 2004;23(4): 501–509. ISSN: 0278-0062. doi: 10.1109/TMI.2004.825627.
22. DRIVE: Digital Retinal Images for Vessel Extraction. [Accessed June 08, 2017]. Available from: http://www.isi.uu.nl/Research/Databases/DRIVE/.
23. Odstrčilík J, Jan J, Gazárek J, Kolář R. Improvement of Vessel Segmentation by Matched Filtering in Colour Retinal Images. World Congress on Medical Physics and Biomedical Engineering, September 7 - 12, 2009, Munich, Germany: Vol. 25/11 Biomedical Engineering for Audiology, Ophthalmology, Emergency & Dental Medicine. Ed. by O Dössel, WC Schlegel. Berlin, Heidelberg: Springer Berlin Heidelberg, 2009; 327–330. ISBN: 978-3-642-03891-4. doi: 10.1007/978-3-642-03891-4_87.
24. HRF: High-Resolution Fundus Image Database. [Accessed June 08, 2017]. Available from: https://www5.cs.fau.de/research/data/fundus-images/.
25. Decencière E, Zhang X, Cazuguel G, Lay B, Cochener B, Trone C, et al. Feedback on a publicly distributed image database: the MESSIDOR database. Image Analysis & Stereology, 2014;33(3): 231–234. ISSN: 1854-5165. doi: 10.5566/ias.1155.
26. MESSIDOR: Methods to evaluate segmentation and indexing techniques in the field of retinal ophthalmology. [Accessed June 08, 2017]. Available from: http://www.adcis.net/en/Download-Third-Party/Messidor.html.
27. Lowell J, Hunter A, Steel D, Basu A, Ryder R, Fletcher E, et al. Optic nerve head segmentation. IEEE Transactions on Medical Imaging, Feb. 2004;23(2): 256–264. ISSN: 0278-0062. doi: 10.1109/TMI.2003.823261.
28. ONHSD: Optic Nerve Head Segmentation Dataset. [Accessed June 08, 2017]. Available from: http://reviewdb.lincoln.ac.uk/Image%20Datasets/ONHSD.aspx.
29. Al-Diri B, Hunter A, Steel D, Habib M, Hudaib T, Berry S. REVIEW - A reference data set for retinal vessel profiles. 2008 30th Annual International Conference of the IEEE Engineering in Medicine and Biology Society. Aug. 2008; 2262–2265. doi: 10.1109/IEMBS.2008.4649647.
30. REVIEW: Retinal Vessel Image set for Estimation of Widths. [Accessed June 08, 2017]. Available from: http://reviewdb.lincoln.ac.uk/REVIEWDB/REVIEWDB.aspx.
31. Kauppi T, Kalesnykiene V, Kamarainen J-K, Lensu L, Sorri I, Uusitalo H, et al. DIARETDB0: Evaluation Database and Methodology for Diabetic Retinopathy Algorithms. Available from: http://www.it.lut.fi/project/imageret/diaretdb0/doc/diaretdb0_techreport_v_1_1.pdf.

32. DIARETDB0: Standard Diabetic Retinopathy Database Calibration level 0. [Accessed June 08, 2017]. Available from: http://www2.it.lut.fi/project/imageret/diaretdb0/.
33. Niemeijer M, Ginneken B van, Cree MJ, Mizutani A, Quellec G, Sanchez CI, et al. Retinopathy Online Challenge: Automatic Detection of Microaneurysms in Digital Color Fundus Photographs. IEEE Transactions on Medical Imaging, Jan. 2010;29(1): 185–195. ISSN: 0278-0062. doi: 10.1109/TMI.2009.2033909.
34. ROC: Retinopathy Online Challenge Database. [Accessed June 08, 2017]. Available from: http://webeye.ophth.uiowa.edu/ROC/.
35. Kauppi T, Kalesnykiene V, Kamarainen J-K, Lensu L, Sorri I, Raninen A, et al. DIARETDB1 diabetic retinopathy database and evaluation protocol. Available from: http://www.it.lut.fi/project/imageret/diaretdb1/doc/diaretdb1_techreport_v_1_1.pdf.
36. DIARETDB1: Standard Diabetic Retinopathy Database Calibration level 1. [Accessed June 08, 2017]. Available from: http://www2.it.lut.fi/project/imageret/diaretdb1/.
37. Decencière E, Cazuguel G, Zhang X, Thibault G, Klein J-C, Meyer F, et al. TeleOphta: Machine learning and image processing methods for teleophthalmology. IRBM, 2013;34(2): Special issue: ANR TECSAN: Technologies for Health and Autonomy, 196 –203. ISSN: 1959-0318. doi: 10.1016/j.irbm.2013.01.010.
38. e-ophtha: A Color Fundus Image Database. [Accessed June 08, 2017]. Available from: http://www.adcis.net/en/Download-Third-Party/E-Ophtha.html.
39. Hoover A, Goldbaum M. Locating the optic nerve in a retinal image using the fuzzy convergence of the blood vessels. IEEE Transactions on Medical Imaging, Aug. 2003;22(8): 951–958. ISSN: 0278-0062. doi: 10.1109/TMI.2003.815900.
40. STARE: Structured Analysis of the Retina. [Accessed June 08, 2017]. Available from: http://cecas.clemson.edu/~ahoover/stare/index.html.
41. Niemeijer M, Xu X, Dumitrescu AV, Gupta P, Ginneken B van, Folk JC, et al. Automated Measurement of the Arteriolar-to-Venular Width Ratio in Digital Color Fundus Photographs. IEEE Transactions on Medical Imaging, Nov. 2011;30(11): 1941–1950. ISSN: 0278-0062. doi: 10.1109/TMI.2011.2159619.
42. INSPIRE: Iowa Normative Set for Processing Images of the Retina. [Accessed June 08, 2017]. Available from: http://medicine.uiowa.edu/eye/inspire-datasets.
43. Vázquez SG, Cancela B, Barreira N, Penedo MG, Rodríguez-Blanco M, Pena Seijo M, et al. Improving retinal artery and vein classification by means of a minimal path approach. Machine Vision and Applications, 2013;24(5): 919–930. ISSN: 1432-1769. doi: 10.1007/s00138-012-0442-4.
44. VICAVR Database. [Accessed June 08, 2017]. Available from: http://www.varpa.es/research/ophtalmology.html#databases.
45. Ortega M, Penedo MG, Rouco J, Barreira N, Carreira MJ. Retinal Verification Using a Feature Points-based Biometric Pattern. EURASIP Journal on Advances in Signal Processing - Special issue on recent advances in biometric systems: a signal processing perspective, Jan. 2009;2009, 2:1–2:13. ISSN: 1110-8657. doi: 10.1155/2009/235746.
46. VARIA. [Accessed June 08, 2017]. Available from: http://www.varpa.es/research/biometrics.html#databases.
47. FIRE: Fundus Image Registration Dataset. [Accessed June 08, 2017]. Available from: http://www.ics.forth.gr/cvrl/fire.
48. Adal KM, Etten PG van, Martinez JP, Vliet LJ van, Vermeer KA. Accuracy asessment of intra- and intervisit fundus image registration for diabetic retinopathy screening. Investigative Ophthalmology & Visual Science, 2015;56(3): 1805–1812. doi: 10.1167/iovs.14-15949.
49. RODREP: Rotterdam Ophthalmic Data Repository Longitudinal diabetic retinopathy screening data. [Accessed June 8, 2017]. Available from: http://www.rodrep.com/longitudinal-diabetic-retinopathy-screening---description.html.
50. Stewart CV, Tsai C-L, Roysam B. The dual-bootstrap iterative closest point algorithm with application to retinal image registration. IEEE Transactions on Medical Imaging, Nov. 2003;22(11): 1379–1394. ISSN: 0278-0062. doi: 10.1109/TMI.2003.819276.

51. Tsai CL, Li CY, Yang G, Lin KS. The Edge-Driven Dual-Bootstrap Iterative Closest Point Algorithm for Registration of Multimodal Fluorescein Angiogram Sequence. IEEE Transactions on Medical Imaging, Mar. 2010;29(3): 636–649. ISSN: 0278-0062. doi: 10.1109/TMI.2009.2030324.
52. Chen J, Tian J, Lee N, Zheng J, Smith RT, Laine AF. A Partial Intensity Invariant Feature Descriptor for Multimodal Retinal Image Registration. IEEE Transactions on Biomedical Engineering, July 2010;57(7): 1707–1718. ISSN: 0018-9294. doi: 10.1109/TBME.2010.2042169.
53. Zheng J, Tian J, Deng K, Dai X, Zhang X, Xu M. Salient Feature Region: A New Method for Retinal Image Registration. IEEE Transactions on Information Technology in Biomedicine, Mar. 2011;15(2): 221–232. ISSN: 1089-7771. doi: 10.1109/TITB.2010.2091145.
54. Ghassabi Z, Shanbehzadeh J, Sedaghat A, Fatemizadeh E. An efficient approach for robust multimodal retinal image registration based on UR-SIFT features and PIIFD descriptors. EURASIP Journal on Image and Video Processing, 2013;2013(1): 1–16. ISSN: 1687-5281. doi: 10.1186/1687-5281-2013-25.
55. Hernandez M, Medioni G, Hu Z, Sadda S. Multimodal Registration of Multiple Retinal Images Based on Line Structures. 2015 IEEE Winter Conference on Applications of Computer Vision. Jan. 2015; 907–914. doi: 10.1109/WACV.2015.125.
56. Hernandez-Matas C, Zabulis X, Argyros AA. Retinal image registration based on keypoint correspondences, spherical eye modeling and camera pose estimation. 2015 37th Annual International Conference of the IEEE Engineering in Medicine and Biology Society (EMBC). Aug. 2015; 5650–5654. doi: 10.1109/EMBC.2015.7319674.
57. Hernandez-Matas C, Zabulis X, Triantafyllou A, Anyfanti P, Argyros AA. Retinal image registration under the assumption of a spherical eye. Computerized Medical Imaging and Graphics, 2017;55. Special Issue on Ophthalmic Medical Image Analysis, 95–105. ISSN: 0895-6111. doi: 10.1016/j.compmedimag.2016.06.006.
58. Hernandez-Matas C, Zabulis X, Argyros AA. Retinal image registration through simultaneous camera pose and eye shape estimation. 2016 38th Annual International Conference of the IEEE Engineering in Medicine and Biology Society (EMBC). Aug. 2016; 3247–3251. doi: 10.1109/EMBC.2016.7591421.
59. Lin Y, Medioni G. Retinal image registration from 2D to 3D. Computer Vision and Pattern Recognition, 2008. CVPR 2008. IEEE Conference on. June 2008; 1–8. doi: 10.1109/CVPR.2008.4587705.
60. Legg P, Rosin P, Marshall D, Morgan J. Improving accuracy and efficiency of mutual information for multi-modal retinal image registration using adaptive probability density estimation. Computerized Medical Imaging and Graphics, 2013;37(7–8): 597 –606. ISSN: 0895-6111. doi: 10.1016/j.compmedimag.2013.08.004.
61. Reel PS, Dooley LS, Wong KCP, Börner A. Robust retinal image registration using expectation maximisation with mutual information. 2013 IEEE International Conference on Acoustics, Speech and Signal Processing. May 2013; 1118–1122. doi: 10.1109/ICASSP.2013.6637824.
62. Gharabaghi S, Daneshvar S, Sedaaghi MH. Retinal Image Registration Using Geometrical Features. Journal of Digital Imaging, 2013;26(2): 248–258. ISSN: 1618-727X. doi: 10.1007/s10278-012-9501-7.
63. Perez-Rovira A, Cabido R, Trucco E, McKenna SJ, Hubschman JP. RERBEE: Robust Efficient Registration via Bifurcations and Elongated Elements Applied to Retinal Fluorescein Angiogram Sequences. IEEE Transactions on Medical Imaging, Jan. 2012;31(1): 140–150. ISSN: 0278-0062. doi: 10.1109/TMI.2011.2167517.
64. Lowe DG. Distinctive Image Features from Scale-Invariant Keypoints. International Journal of Computer Vision, 2004;60(2): 91 –110. ISSN: 1573-1405. doi: 10.1023/B:VISI.0000029664.99615.94.
65. Bay H, Ess A, Tuytelaars T, Gool LV. Speeded-Up Robust Features (SURF). Computer Vision and Image Understanding, 2008;110(3): Similarity Matching in Computer Vision and Multimedia, 346 –359. ISSN: 1077-3142. doi: 10.1016/j.cviu.2007.09.014.
66. Babenko B, Yang MH, Belongie S. Robust Object Tracking with Online Multiple Instance Learning. IEEE Transactions on Pattern Analysis and Machine Intelligence, Aug. 2011;33(8): 1619–1632. ISSN: 0162-8828. doi: 10.1109/TPAMI.2010.226.

67. Yang G, Stewart CV, Sofka M, Tsai CL. Registration of Challenging Image Pairs: Initialization, Estimation, and Decision. IEEE Transactions on Pattern Analysis and Machine Intelligence, Nov. 2007;29(11):1973–1989. ISSN: 0162-8828. doi: 10.1109/TPAMI.2007.1116.